Predictive Modelling and Optimization of the Mechanical Properties of Laser-Coated NB/SiC/Ni Welds Using an ANFIS

Zhe Zou , Juan Chen , Ming-Der Jean *

Posted Date: 18 April 2024

doi: 10.20944/preprints202404.1249.v1

Keywords: SiC/BN/Ni welds; ANFIS; hardness properties; metal-matrix composite; laser cladding

Article

Predictive Modelling and Optimization of the Mechanical Properties of Laser-Coated NB/SiC/Ni Welds Using an ANFIS

Zhe Zou, Juan Chen and MingDer Jean *

College of Arts and Design, Jimei University, 185 Yinjiang Rd., Jimei District, Xiamen 361021, China
* Correspondence: mdjeam@foxmail.com

Abstract: In the present work, a predictive modelling and optimization with the adaptive network based fuzzy inference system (ANFIS) modelling of mechanical properties of laser-coated NB/SiC/Ni welds was studied based on Taguchi design by laser cladding. An ANFIS model based on a Sugeno type fuzzy inference system was developed for predicting the hardness properties of SiC/BN/Ni welds by laser cladding with experimental data required for network training and prediction. Based on analysis of variance, three important factors were taken as inputs for the fuzzy logic inferences, while the hardness properties were taken as the output of the ANFIS. The microstructure of welds were analysed using scanning electron microscopy with an energy dispersive X-Ray spectrometer. Highly developed leaf-like dendrites and eutectic crystals were found in some areas of the melting zone for the BN/SiC/Ni weld, which was significantly hardened. The ANFIS model based on Taguchi's design provides a better pattern of response because the predicted and experimental values were highly similar. As a result, a satisfactory result was achieved between the predicted and experimental values of hardness in laser-coated NB/SiC/Ni welds, whereby the success and validity of the method was verified.

Keywords: SiC/BN/Ni welds; ANFIS; hardness properties; metal-matrix composite and laser cladding

1. Introduction

The protective capabilities of metal-matrix composite coatings for hard-surface environments with high temperature, wear, corrosion, impact and fatigue resistance have been of great interest in industrial applications, especially in the areas of cutting tools, turbine blades, engine valves, and so on. Recently, there has been a great deal of interest in the use of ceramic-matrix composites including carbides, nitrides and borides on steel and non-ferrous alloys, because of their integrated properties, which have proved to be an excellent protective material in additive manufacturing [1,2]. These hard alloys can be effectively used to improve the mechanical properties of metal-matrix composites. Silicon carbide alloys, with their high melting point and high hardness, are of great significance for sandpaper, grinding wheels, and cutting tools, where they have long been used by manufacturers for equipment such as bearings in high-temperature environments, heated machine parts, automotive brakes, and even knife-sharpening tools [3–7]. Therefore, they are widely used in harsh environments such as high temperature, abrasion, corrosion, shock and fatigue [8–10]. But, silicon carbide alloys are high in hardness and brittleness, which make them difficult to machine. A number of disadvantages of silicon carbide have been noted, including reduced strength, non-uniform distribution, thermal stress concentration and crack formation, particularly in high volume fraction silicon carbide coatings, thus limiting the application of silicon carbides. Therefore, typical silicon carbide alloys are hardly able to meet the requirements of workpieces in harsh working environments [11–13]. With these challenges, various surface strengthening techniques have been investigated, containing metal matrix composites with transition alloys and intermediates because of their good

 doi:10.20944/preprints202404.1249.v1

wettability and ductility. Many of the existing publications have addressed the use of transition alloy materials for manufacturing metal-ceramic coatings by using laser cladding [18,19]. These transition alloys are equipped with a binder phase that protects the carbide from oxidation and decomposition [20–25]. They add binder phase materials to form metal-ceramic composite layers by laser cladding, which reduces the structural defects of highly brittle carbides during the cladding process. For example, Li et al. investigated the fabrication of mirrors made of silicon-carbide ceramics by additive manufacturing methods using material extrusion and laser cladding. The experimental results show that optical elements of silicon carbide with more complex structures can be manufactured, which is difficult to achieve with conventional ceramic moulding and sintering techniques [26]. Li et al. developed the microstructure, the mechanism of formation and the properties of Ti+SiC based on the Ti6Al4V substrate by laser cladding [27]. Yin et al. conducted hierarchical porous SiCnw-Si3N4 composite ceramics with good electromagnetic absorption properties. An increase in solid loading decreased apparent porosity and improved flexural strength and fracture toughness [28]. Zhou et al. studied the preparation of carbon fibre reinforced Si3N4 ceramics with pyrolytic carbon (PyC)/SiC interphase by gel casting method. The results showed that the chemical compatibility between carbon fibres and Si3N4 matrix at high temperature was significantly improved by the introduction of PyC/SiC phase [29]. Mazumder et al. studied a series of Si3N4-SiCnw and MgF2-added Si3N4-SiCnw composites that were manufactured at 1650°C using hot press sintering [30]. Lusquiños et al. examined the laser melting of SiC/Si composite coatings on Si-SiC ceramic substrates. The results showed that the use of SiC+SiO2 mixed powders caused serious damage to the substrate material, while the use of SiC+Si mixed powders resulted in good coatings without causing damage to the substrate [31]. Zheng et al. depicted the microstructure and wear properties of laser clad Al+SiC powders on AZ91D magnesium alloy. The results show that the surface hardness of the cladding layer is higher than that of the substrate which increased with the increase of SiC content in the cladding layer. Meanwhile, the in situ synthesised SiC particle composite coatings significantly improved the wear resistance [32]. Sun et al. focused on the preparation process of BN materials and the application of BN composite coatings, in which h-BN has outstanding physical and chemical properties [33]. Based on the above literature, many studies have shown that the use of binder phase additives in metal matrix composites in highly hard environments has the potential to ameliorate the susceptibility of ceramic-reinforced coatings to laser cladding, whereas much of the research on ceramic-metal composites has been directed towards the characterisation of silicon carbide composites in one binder phase. However, studies on the mechanical properties of transition alloys and intermediates both used in metal-matrix composites, especially in silicon carbide composites, are still limited [34–39]. Silicon carbide is very hard to be coated because of its susceptibility to sublimation at high temperatures. Therefore, it is desirable to extend some useful transition and intermediate alloys to high carbon silicon which can be further explored in depth to improve the properties of silicon carbide composites. In this study, the introduction of layered structural dispersants such as boron nitride and nickel-based alloys into silicon carbide composites that can enhance the properties of ceramic-metal silicon carbide composites based on the concept of weak boundary phase of carbide. Moreover, the influence and relationship of process parameters on mechanical properties, such as modelling, cannot be studied systematically and accurately. However, the laser cladding process and cemented carbide composites both are highly nonlinear, multivariate, strongly coupled, and complex processes with large stochastic uncertainties that often require empirical decisions with less than optimal results. They are unable to give a full description of the complicated relationship between the data due to its behaviour of dynamic and nonlinearity. There is a need for several new attempts. The uncertainty of ceramic-metal composites is well solved by developing an several predictive models using soft programming technique such as artifcial neural network, fuzzy-logic, adaptive network-based fuzzy inference system etc so that the complex welding problems, such as parameter-property relationships, predicting and monitoring the quality of welded joints, designing welding process parameters, controlling weld shaping, tracking weld beads and detecting welding defects, can be solved [40–51]. There are, however, some drawbacks to them, such as poor global search capability and long training time. Furthermore, fuzzy logic

 doi:10.20944/preprints202404.1249.v1

interference systems rely on the knowledge and experience of professional experts, which makes it difficult to obtain satisfactory results in the lack of information in knowledge databases. [52–59]. Therefore, the above discussion leads us to propose an improved adaptive neuro-fuzzy inference system in this paper. This is because that it is a hybrid AI technique, which is the combination of fuzzy logic and artificial neural networks. The ANFIS integrates the advantages of the fuzzy inference system, which is easily expressed in fuzzy linguistic terms, with the self-learning ability of artificial neural networks by giving full use of their strengths. Although optimisation and modelling of metal-ceramic composites applied to welding processes has been reported in the literature. However, the optimisation and modelling of the properties of BN/SiC/Ni welds by laser cladding that uses ANFIS in Taguchi's method do not appear to have been reported.

In this study, ceramic-metal composite coatings on substrates by laser cladding are investigated by applying artificial intelligence which aims to provide a valuable insight into the mechanical properties of BN/SiC/Ni coatings. The mechanical properties of BN/SiC/Ni coatings are improved by optimization design and artificial intelligence, which an ANFIS algorithm based on Taguchi's experiments is developed to model the hardness behaviour of the coatings. The influence of microstructural evolution, hardness properties and modelling of BN/SiC/Ni coatings with different parameters in laser welding is analysed. Furthermore, the hardness properties of laser BN/SiC/Ni welds are modelled using the ANFIS based on the parametric design to understand the response pattern of experimental domain. A better understanding of the hardness properties is gained through the prediction of ANFIS, which allowed us to know the effect of various variables on hardness by simulating the hardening behaviour of BN/SiC/Ni welds.

2. Experimental Design and Analysis

2.1. Materials and Preparations

The experimental equipment of laser cladding consists of YLS-3000 fibre laser, six-axis robotic arm, laser water cooler and PLC control system, as shown in Figure 1a. In addition, the laser cladding experiments used the laser via nozzle shown in Figure 1b, where powder 1, a Ni-based powder, and powder 2, a BN-based powder, are mixed in a mixing chamber using nitrogen, which is coaxially fed to the SiC powder pre-positioned on the substrate to produce a fused layer, resulting in a BN/SiC/Ni weld. Transition metals such as nickel-based and BN-based powders are used in laser cladding that forms silicon carbide composite welds which improve the properties of high hardness silicon carbide. The size of the base metal is 40mm x 20mm x 10mm. The microhardness test was carried out using an AVK-C1 hardometer manufactured by Mitutoyo. The test is carried out on the entire weld bead including the molten zone, heat-affected zone and the base material, with a total of 14 points, while the hardness calculation is mainly measured in the molten zone for modelling calculation. Table 1 lists the BN/SiC/Ni mixtures in this study, where the substrates are 40Cr and #45 steel, the NB powders were 0-30 %, the SiC powder is 70-100%, the Ni powder is 0-30%, the laser power is 2400-2800 W, the carrier flow rate is 1400-1800 ml/min, and the travel speed is 2-6 mm/s and stand-off distance is 40-50 mm.

Table 1. Control factors and their levels for butt joints.

Symbol	Controllable factors	Level 1	Level 2	Level 3
A	Base metal	40Cr steel	#45 steel	-
B	BN(wt%)	0	15	30
C	SiC(wt%)	100	85	70
D	Ni(wt%)	0	15	30
E	Power of laser(W)	2400	2600	2800
F	Carrier gas(mL/min)	1400	1600	1800
G	Travel speed (mm/s)	2	4	6
H	Stand-off distance(mm)	40	45	50

 doi:10.20944/preprints202404.1249.v1

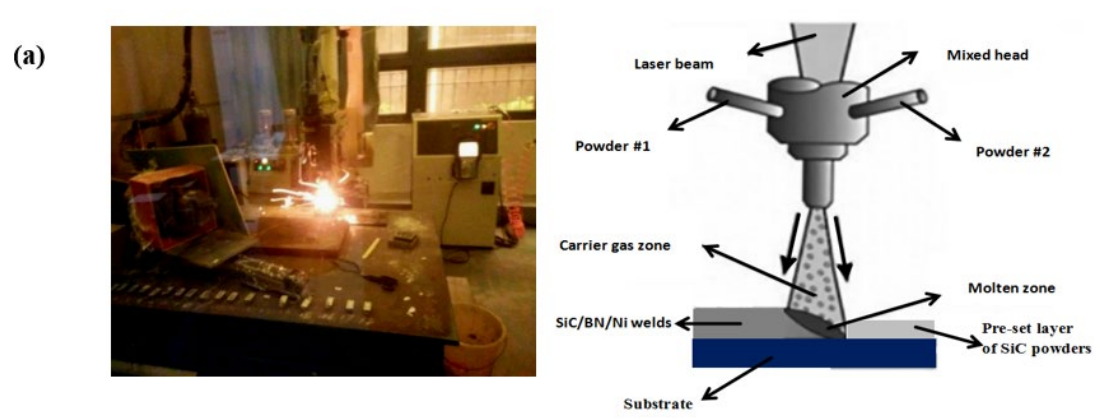

Figure 1. (a) The process of laser cladding used in this work (b) Enlarged schematic diagram of the operation of laser cladding of a specimen.

2.2. Experimental Design and Layout

With laser cladding, a number of controlled variables are required to minimize unwanted defects in the weld. If the variables are chosen poorly, voids, cracks, and dissolved SiC can be generated, leading to weld characteristics that cannot be controlled. However, the variables of laser cladding come to play significant roles in the behavior of the weld. This is because the laser cladding process involves many variables that affect the properties of the weld. Therefore, the variables of laser cladding must be controlled. A total of 18 experiments were conducted while using a two-and-three layer array of L18 orthogonal tables that could accommodate many design factors simultaneously to obtain sufficient experimental information. Table 1 shows the control factors and the level of each factor in the Taguchi design, where one 2-factor and seven 3-level factors containing A, B, C, D, E, F, G and H were allocated to the orthogonal arrays. It is a matrix of fractional factors that ensures a balanced comparison of the levels of any factor or interaction between factors. These factors and their alternative levels that were used in the experiment are listed in Table 2. In this study, The Taguchi method provides minimal sensitivity to various causes of variation, and optimizes control parameters by using orthogonal arrays over the entire parameter space, thereby yielding high-quality products with development and manufacturing costs. In order to evaluate the influence of factors on the response, Taguchi suggests using a special form of response transformation called signal-to-noise ratio (S/N), which measures quality with emphasis on variation [26]. In this study, the logarithmic transformation was used for the smaller-the-better case, such as the wear volume for cladding welds. The S/N ratio based on the loss functions is calculated from Equation (1):

$$\eta = -10Log\left[\frac{1}{n}\left(\sum_{i=1}^{n} 1/y_i^2\right)\right] \quad (1)$$

where $\bar{y}_i$ is the mean and S_i is the standard deviation of the i^{th} trial, m is the predefined value of 18 trails, which is measured in decibels. The S/N ratio was calculated, and the mean and standard deviation of each variable are summarized in Table 2. Each trial was repeated three times for wear volume, which was analyzed for rank order and maximal values using mean value analysis with signal-to-noise ratio, ANOVA was also used again to determine the significant factors for each quality characteristic. Subsequently, predictions of quality characteristics were made using these factors incorporated into the ANFIS model.

 doi:10.20944/preprints202404.1249.v1

Table 2. An orthogonal array with six parameters, three levels and the observed response by laser cladding.

									Microhardness (HV)					S/N ratio
EXP	A	B	C	D	E	F	G	H	H1	H2	H3	Mean	St.Dev	(dB)
1	1	1	1	1	1	1	1	1	423	442	440	434.9	8.5	52.77
2	1	1	2	2	2	2	2	2	437	434	472	447.6	17.2	53.02
3	1	1	3	3	3	3	3	3	478	479	500	485.7	10.2	53.73
4	1	2	1	1	2	2	3	3	367	386	377	376.8	7.8	51.52
5	1	2	2	2	3	3	1	1	431	453	443	442.3	9.0	52.91
6	1	2	3	3	1	1	2	2	596	589	626	603.5	15.8	55.61
7	1	3	1	2	1	3	2	3	484	499	488	490.4	6.3	53.81
8	1	3	2	3	2	1	3	1	412	432	424	422.5	8.2	52.52
9	1	3	3	1	3	2	1	2	712	698	754	721.2	23.6	57.16
10	2	1	1	3	3	2	2	1	353	376	380	369.7	11.9	51.36
11	2	1	2	1	1	3	3	2	412	443	442	432.4	14.4	52.72
12	2	1	3	2	2	1	1	3	578	602	609	596.4	13.3	55.51
13	2	2	1	2	3	1	3	2	345	376	348	356.4	13.9	51.04
14	2	2	2	3	1	2	1	3	712	756	796	754.6	34.2	57.55
15	2	2	3	1	2	3	2	1	567	586	575	575.9	7.8	55.21
16	2	3	1	3	2	3	1	2	375	396	382	384.4	8.7	51.70
17	2	3	2	1	3	1	2	3	479	470	528	492.3	25.4	53.84
18	2	3	3	2	1	2	3	1	493	512	529	511.4	14.7	54.18

2.3. Adaptive Network Based Fuzzy Inference System

Adaptive Neuro-Fuzzy Inference System (ANFIS), introduced by Jang in 1993 [52], that has gained remarkable attention from researchers, is a hybrid forecasting model that uses both neural networks and fuzzy logic which is a method for generating mapping relationships between inputs and outputs. ANFIS provides highly efficient models for approximation not only in neuro-fuzzy systems but also in various other machine learning techniques. Thus, the shortcomings of neural network black boxes that are unable to explain decisions and the weaknesses of fuzzy logic where learning relies on personal experience can be overcome. In ANFIS, the learning capabilities and relational structure of artificial neural networks are integrated with the decision-making mechanism of fuzzy logic. ANFIS, like artificial neural networks, utilises a training dataset to achieve sample learning of the rule base in the fuzzy logic system. The prediction of mechanical properties of welding using an ANFIS has the advantages of fast modelling and high prediction accuracy, which provides an effective way to solve the problems of difficult prediction models and low prediction accuracy due to the highly nonlinear nature of the welding process. Figure 2 depicts the architecture of ANFIS. It is deduced from Figure 2 that the network consists of three inputs (X_1, X_2, X_3), where each input is organized by 3 membership functions. In addition, the layer containing 27 fuzzy rules and the output layer are useful at building the model. The number of nodes in the first layer can be calculated as the product of 3 (number of inputs) and 3 (number of fuzzy functions) (9). The number of nodes in the other layers (layers 2-4) is linked to the number of fuzzy rules (27). In Figure 2, the basic structure of the ANFIS model is shown. In this example, a five-layer neural network that simulates the operation of a fuzzy inference system as shown in Figure 3 is used. Figure 2 shows the topology of the proposed ANFIS for the hardness yield. Each node in the same layer of the architecture as shown in Figure 2 has a similar function. Square nodes indicate nodes with adjustable parameters, and circular nodes indicate nodes without adjustable parameters. For more details on the implementation of the ANFIS network, it is refered to the literature [22]. ANFIS uses membership functions for several sets while employing the linear functions of Sugeno type for the rule output. Various types of membership functions (MF)are used, such as triangular, trapezoidal, gaussian, and bell functions. For example of Gaussian type of MF, the mathematical equation is:

Preprints.org (www.preprints.org) | NOT PEER-REVIEWED | Posted: 18 April 2024 doi:10.20944/preprints202404.1249.v1

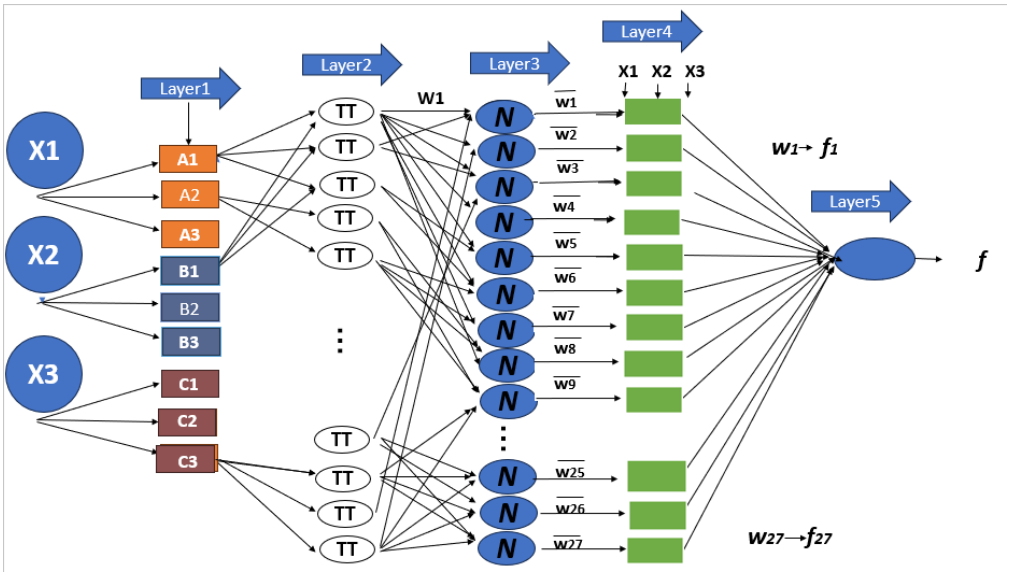

Figure 2. A framework of ANFIS model with five layers including fuzzy membership layer, fuzzification layer, normalisation layer, defuzzification layer and output layer.

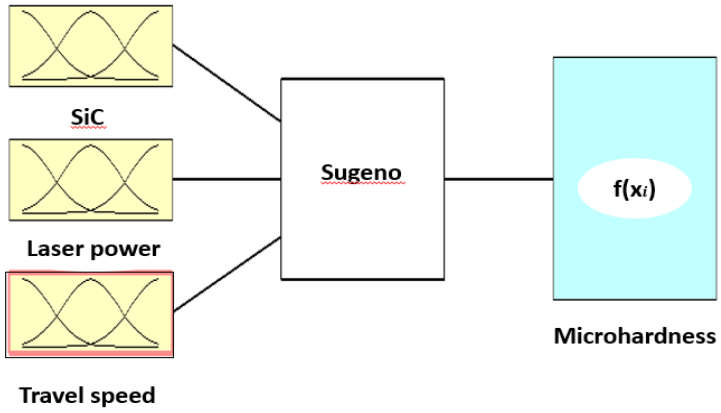

Figure 3. Three inputs and one output fuzzy inference system for laser-coated BN/SiC/Ni welds.

$$\mu(x, a, b, c) = \exp\left[-\left(\frac{x-c}{a}\right)^2\right] \quad (2)$$

where Gauss's one-dimensional graph is the shape of the characteristic symmetric solution "bell curve", where a is the height of the curve's peaks, b is the coordinates of the centre of the peaks, and c is called the standard deviation, which characterises the width of the bell shape. ANFIS has done all the five essential processes of fuzzy control, i.e., input layer, membership layer, fuzzification layer, normalisation layer and defuzzification, which constitute an adaptive neuro-fuzzy system by using a learning algorithm of neural networks that automatically extracts rules from the source data of the input and output samples. Its structure of the model was made by merging adaptive network and fuzzy inference system, which functionally inherited the explainability character of the fuzzy inference system and the learning ability of the adaptive network, which is able to modify the parameters of the system according to the a previous knowledge, so as to make the output of the system closer to the real output. The architecture of the neuro-fuzzy model consists of five unique adaptive layers. Takagi and Sugeno proposed the T-S fuzzy model in 1985. The model was later called Sugeno fuzzy model. It is a nonlinear model that expresses the dynamic properties of complex systems and is the most commonly used fuzzy inference model. Figure 3 shows a neural network

 doi:10.20944/preprints202404.1249.v1

with five layers in which the ANFIS model was trained. The input values, such as SiC, laser power and travel speed, are converted to fuzzy values by means of a membership function. A example of a simple fuzzy inference system, a first-order model of fuzzy Sugeno that is a typical rule base, which contains two If-Then rules can be expressed as follows

$$\text{Rule}_i: \quad \text{If } x_1 \text{ is } A_{1s}, x_2 \text{ is } B_{1s}, \ldots, \text{ and } x_s \text{ is } C_{is}; \text{ then } y_i = f(x_1, x_2, \ldots, x_n) \qquad i=1,2,\ldots,M \tag{3}$$

where x_i (i=1,2,..,s)is the antecedent input, A_{1s}, B_{1s}, and C_{1s} are membership function and $f(x_1,x_2,\ldots,x_s)$ represents the outputs in the consequent part. Typically $y_i=f(x_1,x_2,\ldots,x_s)$ is a polynomial. The following is a brief description of the Sugeno first-order model with two input variables.

Layer 1: The inputs x_1, x_2, x_3 are fuzzified by means of a membership function, which is transformed to obtain the degree of membership of the linguistic types A1, A2, A3, B1, B2, B3, C1, C2, C3 (e.g., Large, Medium, Small) in the interval [0,1]. The output of layer 1, O_{ij}, can be expressed as

$$O_{i1} = \mu_{ij}(X_i), i = 1, \ldots, 3, j = 1, \ldots, 3 \tag{4}$$

where μ_{ij} is the j^{th} membership function for the input X_i.

Layer 2: The firing strength of each rule is obtained by multiplying the degrees of membership of each rule;the weight functions *wi* for the next layer is defined.

$$O_{i2} = wi = \mu_{Ai}(x_1)\mu_{Bi}(x_2)\ \mu_{Ci}(x_3),\ i = 1, 2, 3 \tag{5}$$

Layer 3: The firing strength of each rule obtained from layer 2 is normalised to represent the firing weight of that rule in the whole rule base.

$$O_{i3} = \overline{W_l} = \frac{w_i}{\sum_{i=1}^{3} w_i} \quad i = 1, 2, 3 \tag{6}$$

Layer 4: The results of a calculated output of a linear combinator of the input functions using normalised weights.

$$O_{i4} = \overline{w}_i \ f_i \quad i = 1, 2, 3 \tag{7}$$

Layer 5: The output of the calculation is the sum of the results of the linear combination of the normalized weights of each rule.

$$O_{i5} = \sum_{i=1}^{n} \overline{w}_i f_i(x_i) \qquad i = 1,2,3 \tag{8}$$

In this paper, the parameters in the model are classified into premise and outcome parameters, which are learnt by back propagation algorithm with the least squares calculation. Least squares are used in the forward propagation process to evaluate the subsequent parameters, whereas the backward propagation process updates the premise parameters. There are two important steps in executing an ANFIS model which are training and testing the data. The total number of experimental data to be used in constructing the ANFIS model is 36. In this study, 25 training data and 11 test data are used. The Root Mean Square Error (RMSE) function is employed to examine the performance of the training model by applying it to this network. Its computational formula is as follows:

$$RMSE = \sqrt{\frac{1}{M}\sum_{i=1}^{M}(y_i - d_i)^2} \tag{9}$$

where M is the total number of training sample, d_i is the real output value, and y_i is the ANFIS output value in training algorithms.

3. Experimental Results and Discussion

3.1. Experimental Design Based on Orthogonal Array

Table 2 shows the results of the L18 experiments, which were used to evaluate the microhardness of the NB/SiC/Ni alloy welds by calculating the signal-to-noise ratio (S/N) of the experimental values

 doi:10.20944/preprints202404.1249.v1

with standard deviations. In a similar way, the microhardness results of the microhardness tester can also be seen in Figure 2. The experimental results show a significant difference in microhardness compared to the substrate, with an increase of about 2 times or more, which indicates a good hardening effect. The results of the tests on the hardness of various coatings are given in Table 2, where various patterns and EDS analysis of wear can be visualised. The distributions of hardness for tests 4, 9, 13 and 14 were 376.8±7.8 HV, 721.2±23.6 HV, 356.4±13,9HV and 754.6±34.2 HV, respectively, indicating that they were significantly higher than the hardness of the substrate. Comparing the hardness of the cladding layers in 40Cr and #45 steels is 603HV and 606HV respectively. There is almost no difference between the two. Also, in trials 6,9,12 and 14, The hardness values exceeded 600Hv, i.e., the higher the S/N ratio, the more it indicates better hardened properties, while trials 4,10,13 and 16, the hardness value was lower than 400Hv, i.e., the lower the S/N ratio, the more it indicates smaller hardness values. Figure 3 shows the distribution of the lowest and highest microhardness values in 18 groups of BN/SiC/Ni welds for both substrates, including the melting zone, the heat affected zone and the substrate. Three distinct sizes of hardness are shown for the zones such as melted zone, heat affected zone and substrate. The metallographic structures of the three zones of the cladding are in good agreement with each other. It is clear that the addition of SiC increases the microhardness of the coating. The increase in microhardness is mainly attributed to the dissolution of BN and SiC in the liquid phase which results in an increase in the volume fraction of carbon-boride formed during the laser cladding process.

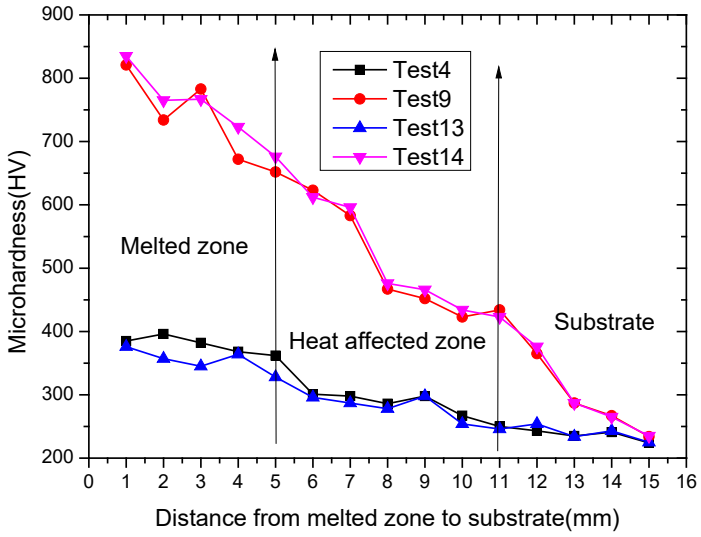

Figure 5. shows the distribution of microhardness values for BN/SiC/Ni welds with tests 4, 9, 13 and 14, including the melting zone, the heat affected zone and the matrix.

3.2. Microstructure of the Weld Zone for Laser-Coated NB/SiC/Ni Welds by Laser Cladding

A magnified 2000X SEM picture of the microstructures in the cross-section of each of the laser-coated NB/SiC/Ni weld can be seen in Figure 3, which shows that the molten zone of the weld is characterised by various sizes of grains. During the laser cladding process, different forms of carbides and precipitates are generated in the composite coatings due to the differences in the carbide, nitride and nickel content of the molten pool. There are large white areas and small black areas in the melting zone, whereas in the lower hardness areas, coarse crystalline with plate-like grains grows, while in the higher hardness areas, the particles are fine with white carbide structure. Unfortunately, this study has failed to avoid partial dissolution of silicon carbide on the molten pool. This is due to the different temperature gradient of the melt pool between the white and dark zones, which affects the corresponding structure of the solidification zone by cladding welds. In addition, Table 2 lists the EDS results for the typical areas labelled Tests 4, 9, 13 and 14 in Figure 3. The powder is pre-positioned on the substrate by laser cladding where the powder is melt-mixed with the substrate. The SEM micrographs of the laser coatings are shown in Figure 3a labeled Test 4, where large grains can be

 doi:10.20944/preprints202404.1249.v1

seen, with plate-like coarse grains growing within the weld zone, along with crystalline structures of Si particles at the grain boundaries. The chemical compositions of the BN/SiC/Ni welds obtained by EDS are listed in Table 3. In EDS, the elements O and Fe are higher, C is lower, and Ni and Si are even lower. The cross-section of the cladding zone shown in Figure 3b indicated Test9 contains obvious black dissolved Si dendrites, no pores and cracks, and irregularly distributed aggregates in the lower-left region, while the white region contains fine precipitated carbides and the lower-right region has some incompletely melted Si. The thickness of the melt layer is about 4-6 μm, which is much smaller than the thicknesses produced by the other fractions. Comparing Figure 3a with Table 2, it is clear that Figure 3b is harder. Furthermore, the EDS analysis shows that Figure 4b has less Si and C elements while more O and Ni elements than Figure 4a. This is due to the different temperature gradients in the melt pool, which affects the solidification time during deposits thereby resulting in different corresponding structures. As shown in Figure 3c, the grain growth is complete, but some of the black particles have not melted and accumulated at the grain boundaries, where pin-like eutectic crystals can be seen in the grains, as shown in the white part of the SEM micrograph. Typical areas labelled Test 13 in Figure 4c and the EDS results are shown in Table 3. An analysis of the distribution of elements in the melting zone by X-ray diffraction shows that the white areas are rich in O and Fe, while C, Si and Ni are less abundant, mainly iron oxide (Fe_2O_3), h-BN, γ-(Ni, Fe), B_4C and iron silicide (Fe_2Si) [12]. As shown in Figure 3d, most of the plate-like carbides and a few unmelted SiC and BN particles are clearly visible in the zone, which contains iron clusters in grey colour and precipitated carbides when melted. It is the hardest of the 18 groups. Table 3 analyses of test 14 using EDS. The analysis of test 14 by EDS is shown in Table 2. In the molten region, O decreases to 5,250% and Ni increases to 1.050, while the remaining elements show little change, which is not evidenced by the EDS analysis. Therefore, it seems to be necessary to use the microstructure of the molten zone as a support for the results.

Table 3. The chemical composition of laser-coated SiC/BN/Ni welds by weight percentage (%) of atomic concentration as shown by EDS surface analysis in Figure 7.

No. of trials	Atomic concentration (%)				
	C	O	Si	Fe	Ni
Trial4	5.509	11.820	0.539	81.580	0.551
Trial 9	2.051	24.967	0.383	69.031	3.568
Trial 13	2.746	3.845	0.342	92,651	0.337
Trial14	2.564	5.259	0.516	90.611	1.050

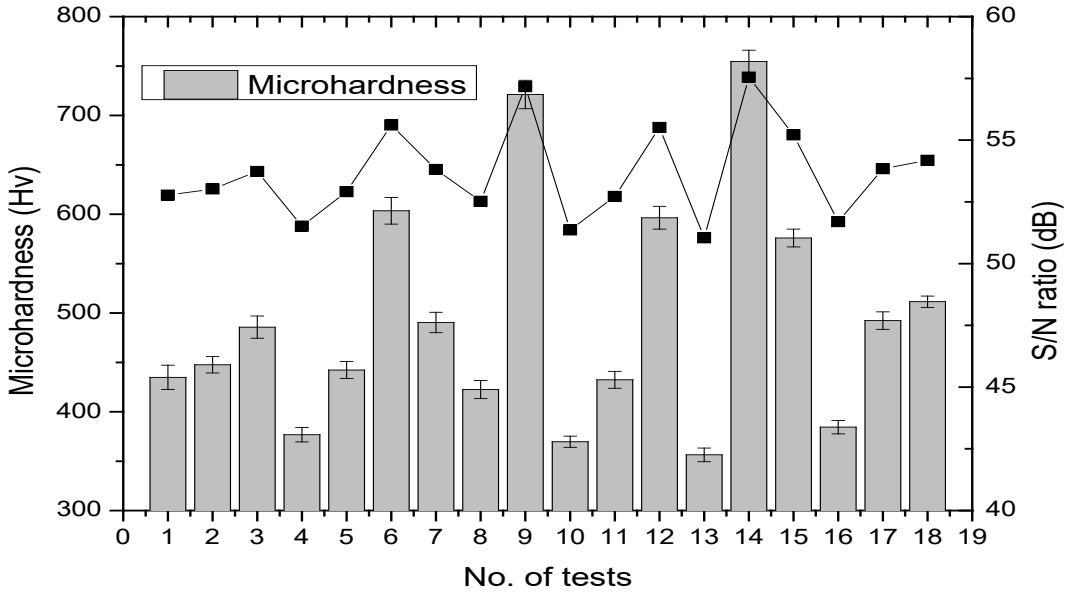

 doi:10.20944/preprints202404.1249.v1

Figure 4. Comparison of signal-to-noise ratio and microhardness with a standard deviation of laser-coated NB/SiC/ Ni welds.

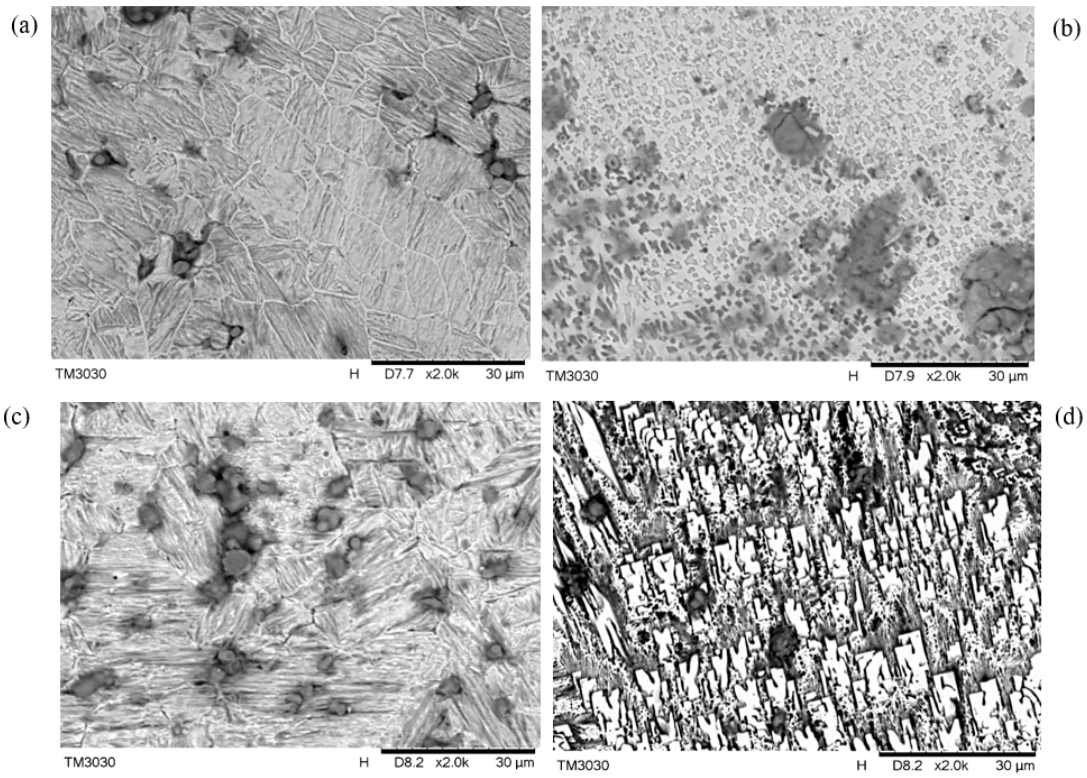

Figure 6. SEM microstructures of various tests in the deposits by laser cladding including (a) trial4;(b) trial9; (c) trial13; (d) trial14.

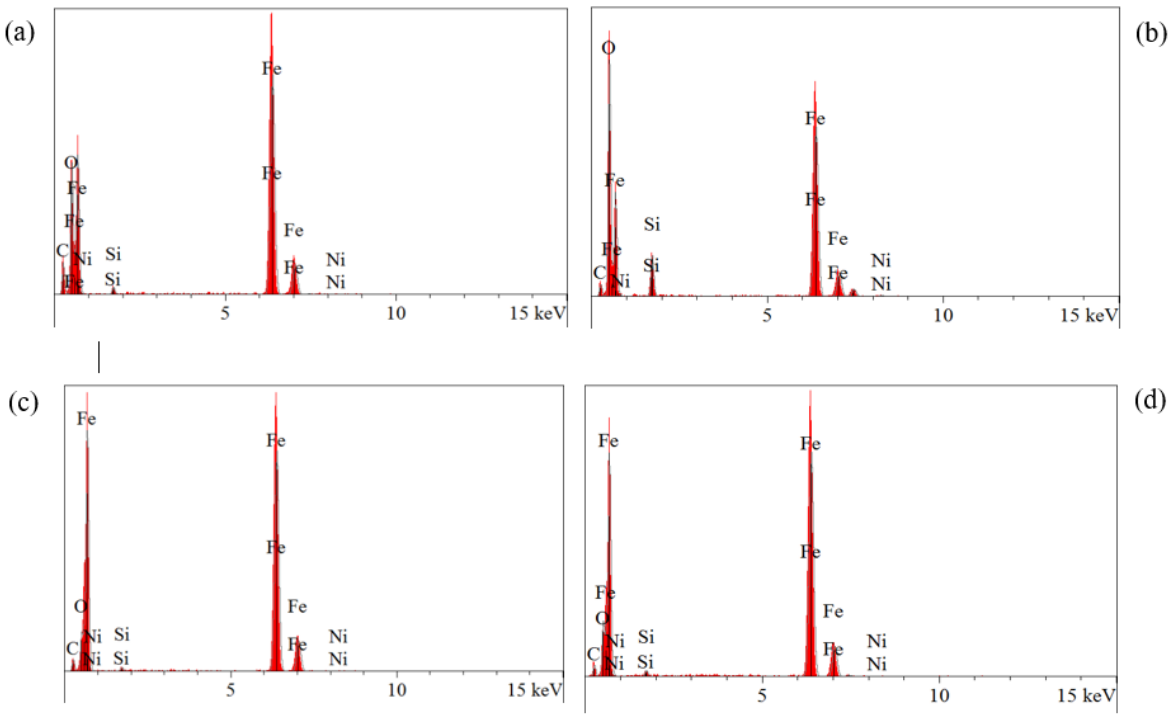

Figure 7. The elemental intensity of the EDS surface analysis with Figure 6 in a laser-coated weld.

 doi:10.20944/preprints202404.1249.v1

3.3. Effect of Designing with Ternary SiC/BN/Ni Mixtures on Hardness Yields

In order to solve the problem of the mixture ratio of three materials using mixture design, it effectively controls the mixture properties of lased cladding. The effects of the three mixture powders, including SiC, BN, and Ni alloys, are considered in turn to determine the relationships between the hardness and the variables and to determine the nature of the hardness. For a better visualization of the effect each component in the three SiC, BN, and Ni blends, the various hypsographic maps using a mixture design are shown in Figure 4, which shows how the three factors (SiC, BN, and Ni) affect the hardness SiC, BN, and Ni response of the clads that yield a desirable value. Figure 4 shows the region of the ternary contour plot which gives an insight into the appropriate proportioning of the three component mixtures of SiC, BN and Ni on the welds of the cladding. As shown in Figure 4a, the triangular response surface to show the effect of SiC, BN, and Ni at fixed control factors and levels for the laser cladding are generated by a linear mixture. The response plots show that hardness is highest with 100% increase in SiC which is decreased slightly with increase in BN. That is, there is a tendency for the upper-left region to have higher hardness, while the lower-right region has lower hardness. Similarity, the plots in Figure 4b show the response surface with contour plots for the effect of SiC, BN, and Ni that are generated by a linear mixture. It displays a contour plot of the hardness using a linear mixture, where the red areas have higher hardness values while the blue areas have lower hardness values. Clearly, the optimum zone of 70–90 wt% SiC 10–30 wt% BN and 10–20 wt% Ni gives the desirable zone for the mixture design. However, the decrease in hardness is due to the addition of proper amounts of Ni element into the WC/Ni/Co blend, but this hardness increases when the amount of SiC powder increases. In summary, there are graphically shown contour areas of linear mixtures which show the desired value of 606HV and a mixture of 67% SiC, 17% BN and 17% Ni was picked. In the triangular contour plot, the area of red highlights is ideal for individual powder components and mixture powder components on the pattern of hardness, which has a greater impact on the expected output for different combinations of mixture components than the other highlight areas.

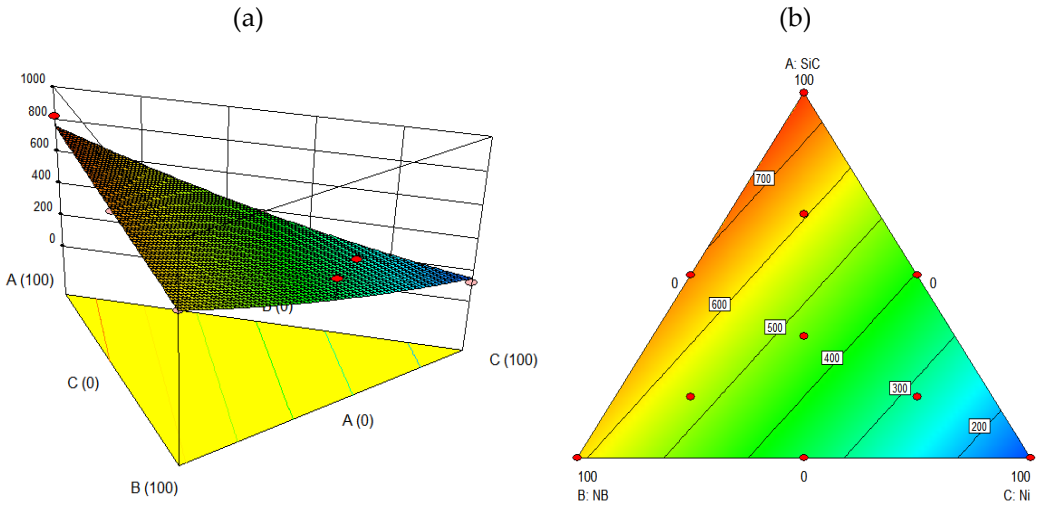

Figure 8. Triangular contour plots for three powder mixed effects with a linear mixture, accounting for the effect of individual and mixture powder components including SiC, BN, and Ni alloys for the hardness. (a) three-dimensional surface plot. (b) contour plot of predicted hardness.

3.4. The Analysis of Variance of Laser-Coated BN/SiC/Ni Welds

The effects of mean values can reflect the importance of the relative performance between each of the control factorial levels. Signal-to-noise ratios are calculated based on the mean values of levels 1, 2, and 3 for each factor in Figure 5. The ranking of the mean response and the effects of the magnitude in the experimental results were evaluated. Their S/N ratio is effective in detecting important factors of laser cladding that affect weld quality. The factors affecting the hardness values

 doi:10.20944/preprints202404.1249.v1

of the laser cladding layers are shown in Table 5. The ordering of the parameters affecting the hardness values is further shown as C, G, E, H, B, F, D and A. also, As seen in Table 5, A_2, B_2, C_3, D_1, E_1, F_2, G_3 and H_3 have the highest S/N values which have the maximal effect on the hardness values, i.e., they are the optimum values. Furthermore, a further analysis of variance based on Equations (10) and (11) was done on Table 5 to validate the significance of the control factors in Table 4. The aim of the analysis of variance (ANOVA) was to investigate the design parameters of laser-coated BN/SiC/Ni welds that have a significant effect on the hardness of the deposit. These contribution rates can be used to assess the importance of each factor to the hardness that is relevant. The total sum of squares, SST, for the ANOVA is:

$$SST = \sum_{i=1}^{n} (Z_i - \overline{Z})^2 \tag{10}$$

where Z_i is the correlated Z response for the i^{th} test, $\overline{Z}$ is the total average of the correlated hardness responses, and n is the number of tests. *SSK* is the sum of squares of the test control factor k, where k = A, B ..... . H, is calculated as

$$SSK = m_k \left[\sum_{j=1}^{m_k} (Z_{K_j} - \overline{Z})^2 \right] \tag{11}$$

where Z_{K_j} is the average response for j^{th} level of Factor k, m_k is the number of repetitions of each level of Factor k. The estimated variance of Factor k, *MSK*, is the ratio of *SSK* to its degrees of freedom (*DOF*), and the estimated variance of random error is so-called the mean squared error, or *MSE*, which is the ratio of *SSE* to its degrees of freedom. Then, the *F-ratio* is simple the ratio of *MSK* to *MSE*. Hence, the ratio (percentage) of contribution of factor *k* is a highly significant indicator for comparing the contribution of factors. That is, the higher the ratio of contribution, the greater the overall variance of the effect is. Table 5 shows the mean squares of the eight control factors, which illustrate the effect of each factor on the variance. Notices that are more important based on the results of Equations (10) and (11) are shown in AVOVA. Compared with the contribution of the error factor (7.62%), we chose the most important SiCwt% (C), laser power (E), and travelling speed (G), while substrate (A), BNwt% (B), Niwt% (D), carrier gas (F), and spacing (H) have smaller percentages, as shown in Table 5. The percentage of explainable variation of these important parameters in the overall is 77.58%. We reconfirmed the most important factors obtained from the average factor analysis in Table 4. These important factors are further incorporated into the ANFIS prediction of the hardness of laser-coated welds.

Table 4. The main effect for S/N ratios during the hardness of welds by laser cladding.

	A	*B*	*C*	*D*	*E*	*F*	*G*	*H*
Level 1	53.67	53.18	52.03	53.87	54.44	53.55	54.60	53.16
Level 2	53.68	53.98	53.76	53.41	53.24	54.13	53.81	53.54
Level 3	0.00	53.87	55.23	53.74	53.34	53.35	52.62	54.33
Effect	0.01	0.79	3.20	0.46	1.19	0.79	1.98	1.17
Rank	8	5	1	7	3	6	2	4

Table 5. An ANOVA table for S/N ratios during the hardness of welds by laser cladding.

Control factors	Sum of squares	Degrees of freedom	Mean square	F-Test ratio	Contribution
A	0.00013	1.0	0.00013	0.00006	0.00
B	2.214	2.0	1.107	0.469	3.57
C	30.794	2.0	15.397	6.528	49.71
D	0.674	2.0	0.337	0.143	1.09

 doi:10.20944/preprints202404.1249.v1

E	5.291	2.0	2.646	1.122	8.54
F	1.996	2.0	0.998	0.423	3.22
G	11.973	2.0	5.987	2.538	19.33
H	4.284	2.0	2.142	0.908	6.92
Error	4.717	2.0	2.359	1.000	7.62
Total	61.944	17.0	3.644		100.00

3.5. Confirm Run and Their Optimization on the Hardness Properties

Three repetitions of each test were carried out in different areas of the melting zone in order to estimate the optimum performance of the welds for all the tests. Table 2 lists the results and the S/N ratios obtained using the formulae that fulfils the " larger-the-better" property. Table 4 shows the computation of the response of the S/N ratio in the orthogonal array experiment using mean value analysis. Clearly, the larger S/N ratio indicates better performance of the laser-coated BM/SiC/BN welds. That is, the higher the S/N ratio, the more important the factor is. As shown in Figure 4, the optimal value for each factor was derived from the maximum S/N value for each level of the factor. The optimal setting for the factorial levels is $A_2B_2C_3D_1E_1F_2G_3H_3$. The optimal parameters for the sputtering process are: substrate of #45 steel, 15wt%BN, 70wt%SiC, 0wt%Ni, laser power of 2400W, carrier gas of 1600 mL/min, travel speed of 6 mm/s, and stand-off distance of 50 mm. Of all the 18 sets of orthogonal array experiments, we choose the 9th group with a pessimistic colour, which is better in the first nine sets, and the 14th group with a dark-blue colour, which is better in the last nine sets, which are compared with the optimal group with a brown colour. As shown in Figure 6, the higher the hardness, the closer it is to the right side of the chart. Using a Gaussian plot, the thinnest solid curve shown on the right side of Figure 6 indicates the best test, which produces the greatest hardness with very little deviation. It is evident that the optimum setting of the control factors is remarkably robust to variability, which demonstrates that reproducibility is good.

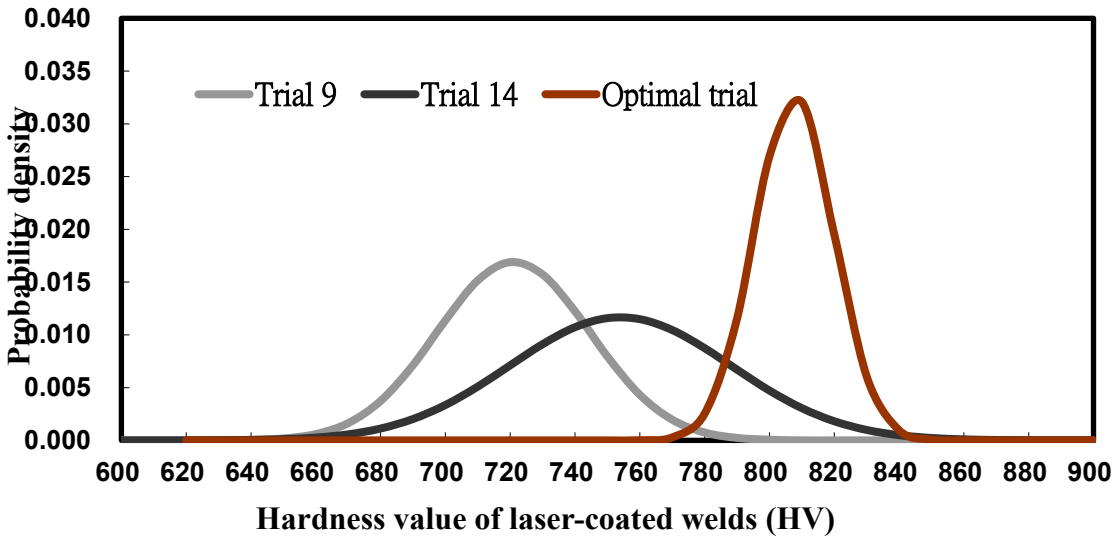

Figure 9. Comparison of probability density for the five trials in the orthogonal table with trial 9, trial 14 and the optimal trial.

4. Results and Discussion

4.1. Analysis of ANFIS Model

In this paper, a predictive model is created using first order TSK type fuzzy rules. Different number of membership functions were tested to find the optimal ANFIS model using a subtractive clustering method. The MATLAB R2021 software package is used. There is, however, the membership function of the Gaussian type that is optimally used. To understand the performance of

 doi:10.20944/preprints202404.1249.v1

ANFIS, Figure 10 shows the prediction of the hardness of the fuzzy system with adaptive network which is executed by passing the three important parameters based on ANOVA such as SiC%, laser power and travel speed by laser coated weld. As shown in Figure 3, the fuzzy logic system has a rule base which contains 3 inputs (SiC%, laser power and travel speed) and 1 output (microhardness). It is applied to the fuzzy logic system that has been trained by the neural network which is shown graphically above the first rule in Figure 10 with a database of 20 rules. By applying logic rules and Mamdani reasoning procedures, multiple logic rules can be triggered to give fuzzy linguistic values for the output response. The model can be used to predict the hardness values of laser-coated welds. For example, the four inputs are SiC (70wt%), laser power(2400W) and travel speed(4mm/s), respectively, whilst the predicted value of microhardness is 603HV. As shown in Figure 11a, training a fuzzy system with a neural network generates a fuzzy layer, a rule base layer, a normalisation layer, an inference layer and a total output layer. Furthermore, the rule base of the fuzzy system is optimised by subtractive clustering method which completes the ANFIS model. As shown in Figure 11b, the results of the root mean square error of the hardness response of the ANFIS model to the training and test data, the fuzzy system was trained by the neural network for 1000 times which resulted in the smallest root mean square error (RMS) of 1.23085 and 1.49378, respectively. Furthermore, the ANFIS predictor fits a distribution curve of the actual data, where the ANFIS prediction and the actual values form a diagonal straight line as shown in Figure 11c,d. The predicted and experimental values are remarkably similar, indicating that the model is reliable. The error for many of the validation tests was less than 3 %, while the maximum error was 9.40 %. However, the distribution of prediction errors for ANFIS fluctuates steadily, with only three prediction errors exceeding the standard deviation of the experimental values by more than 5 %. The comparison of the experimental data with the ANFIS predictions is shown in Figure 12, which verifies that the average error of the ANFIS predictions is 4.625%. It is therefore concluded that the developed ANFIS model provides an effective model for decision makers to predict the hardness characteristics of laser coated BN/SiC/Ni welds.

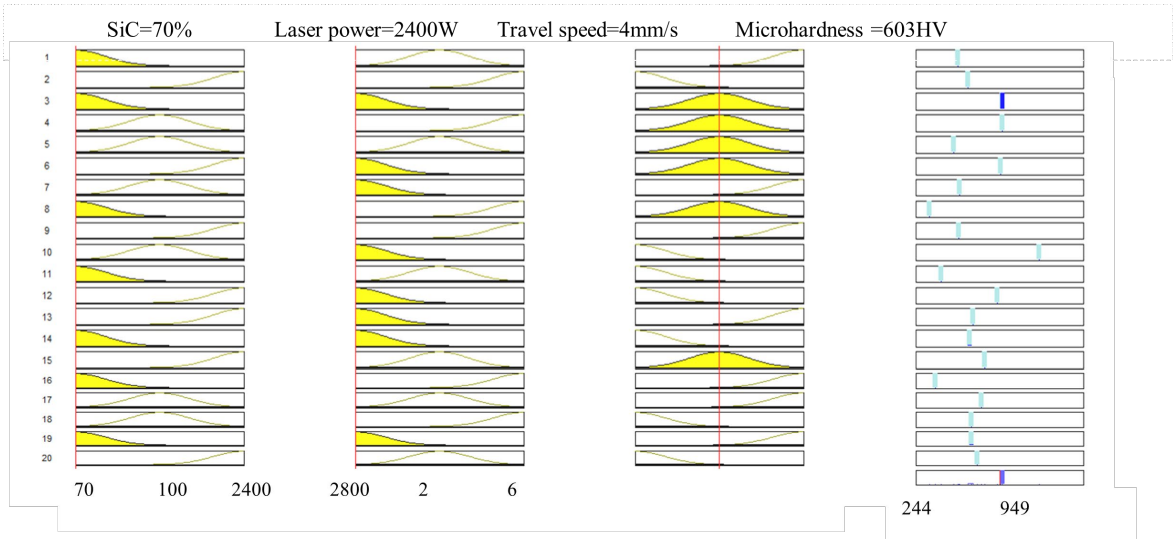

Figure 10. Rule base for fuzzy logic inference using neural network in ANFIS with 3 inputs such as SiC, laser power and travelling speed and 1 output for micro hardness.

Preprints.org (www.preprints.org) | NOT PEER-REVIEWED | Posted: 18 April 2024 doi:10.20944/preprints202404.1249.v1

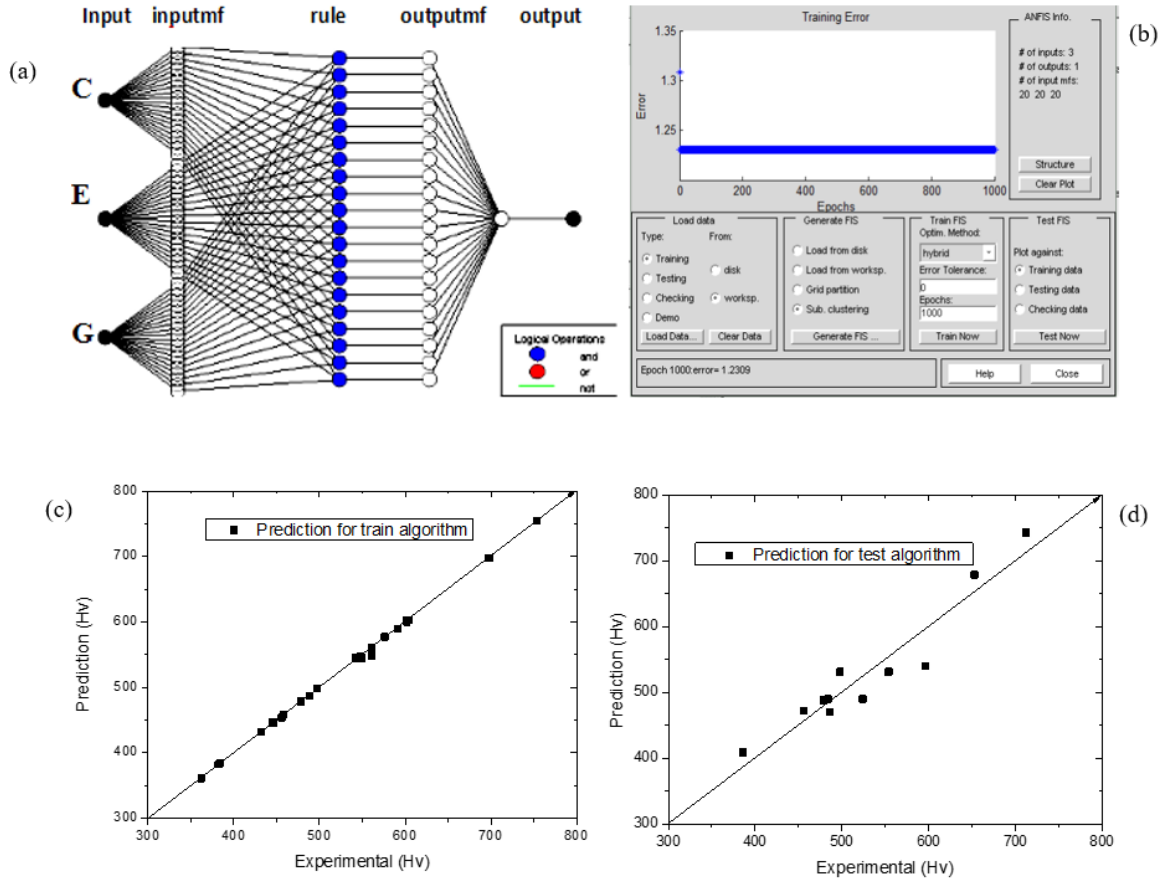

Figure 11. A framework for training of the ANFIS model (a), the error function of the training algorithm (b), and the plot of the training (c) and testing (d) predicted values for the ANFIS model against the experimental values.

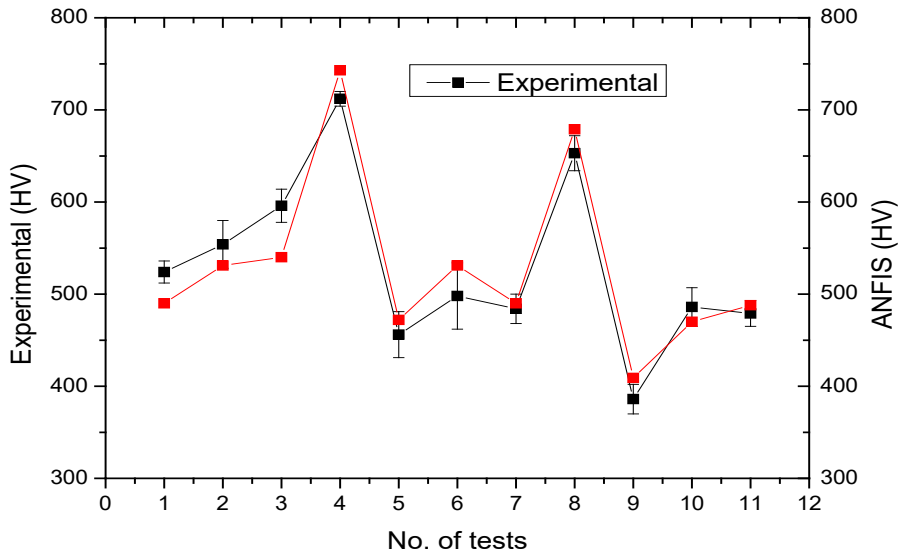

Figure 12. The prediction results of ANFIS model in comparison with the experimental data.

4.5. The Predictor of Surface Response Using an ANFIS

A three-dimensional graph of the prediction is made by using ANFIS model. As shown in Figure 13, the effect of each working parameter on the hardness response can be understood using three

 doi:10.20944/preprints202404.1249.v1

important variables such as SiC, laser power and travel speed based on ANOVA. Figure 13a shows the relationship between hardness with respect to SiC and laser power. At high laser powers near 2800 W, the hardness is 350 HV at the lower level when the SiC is below 10 per cent, while it rises to the higher level of 700 HV when the SiC is near 20 wt%. Meanwhile, the laser power approaching 2600 W and SiC near 20wt% results in a hardness of about 400 HV. As shown in Figure 13b, the hardness is less at a scanning speed of 4-6mm/s when the laser power is 2400w. In addition, when the laser power is in the range of 2500-2700w, the hardness is more than 600 HV, whereas the hardness increases with the increase of laser power to reach more than 700 HV when the scanning speed is nearly 6 mm/s.

(a)

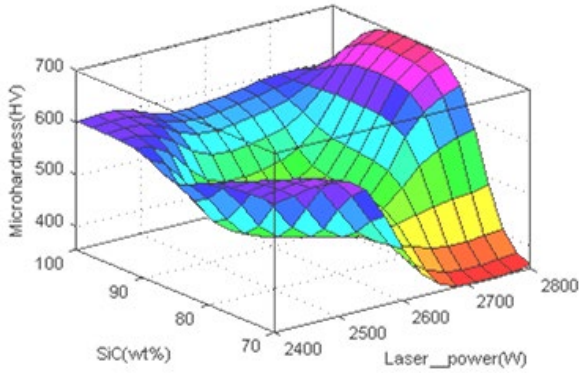

(b)

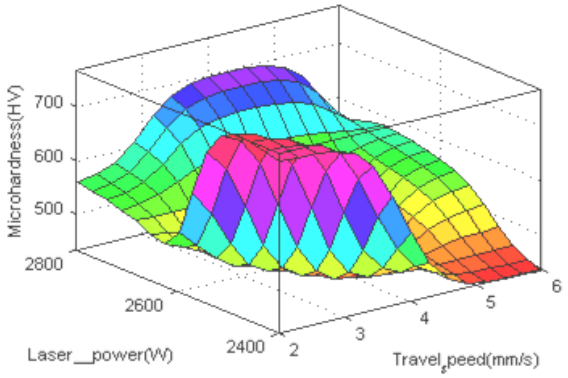

(c)

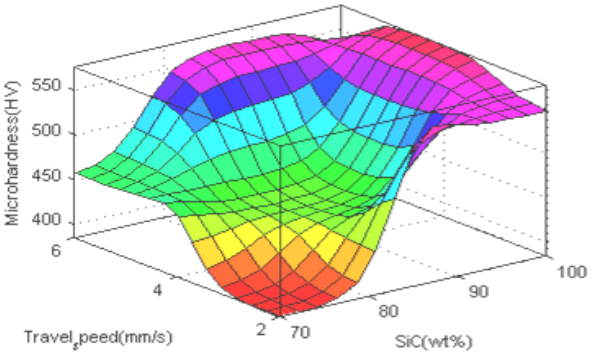

Figure 13. Response surface plots for modelling the hardness yield of laser-coated silicon carbide/boron nitride/nickel welds using the ANFIS model.

As shown in Figure 13c, it is evident that the hardness in relation to ratio of SiC and scanning speed is shown. If both SiC and scanning speed are low, the hardness is relatively lower value at 350 HV. When the travel speed is 2-4mm/s, the hardness rises to 550HV with increasing SiC. Yet, when the travel speed is 5-6mm/s, the hardness rises slowly from 450HV to 550HV with 0-10wt% SiC, and stays at 580-600HV with 10-30wt% SiC. Based on the aforementioned graphs, the corresponding contours show considerable curvature, which indicates that the hardness curvature has a complex nature of correlation with SiC, laser power and Travel speed, which cannot be formulated

 doi:10.20944/preprints202404.1249.v1

mathematically. These graphs show that the larger hardness values mostly fall near the design boundary. Also, it was observed by scanning electron microscopy that the welds at the boundary conditions produced finer structures and harder surface coatings, thus satisfying the desired hardened layer. The above graphs clearly show that it is feasible to understand the relationship between response and variables, whilst at the same time easily characterise the nature of the coatings in the design zone, which can then yield more information about the nature of the cladding system.

5. Concluding Remarks

In this study, the mechanical properties of laser-coated NB/SiC/Ni welds were predicted and optimised based on Taguchi's design using the Adaptive Network for Fuzzy Inference System (ANFIS). Artificial intelligence methods using ANFIS models are available to model the hardness behaviour of welds. By using orthogonal array experiments, the effect of control factors on welds was determined. Based on ANOVA, three important factors such as SiC, laser power and travel speed were used as inputs for fuzzy logic reasoning while hardness properties were used as outputs for ANFIS. The microstructure of the melting zone consists mainly of dendritic crystals, with denser grey areas near the grain boundaries, while the grains in the heat-affected zone are significantly coarsened. Yet, the high-iron zone is mainly composed of iron oxides, borides and a small amount of molten nickel composites for the laser-coated BM/SiC/Ni welds. The difference in hardness attributes compared to the substrate is significant, increasing by a factor of about 4, which indicates good hardness properties. The relationship between important parameters and hardness of laser melting zone was constructed using an ANFIS. An ANFIS model based on the Sugeno type fuzzy inference system was established by using SiC/BN/Ni alloys for laser cladding with the data necessary for network training and prediction, which was used to predict the hardness properties of welded coatings. The algorithm using artificial neural networks with learning abilities by training the network in combination with least squares.The root mean square error (RMSE) obtained for the training data and test data in predicting of hardness response using an ANFIS model was 1.23085 and 1.49378 after 1000 epochs of computation, respectively. Meanwhile, comparison of the experimental data with the ANFIS predictions has verified that the mean error of the ANFIS predictions is 4.625%. The response patterns of the ANFIS clearly show that it is viable to understand the relationship between the response and the variables, while also making it easy to determine the nature of the coating in the design domain. The experimental results of laser cladding of SiC/BN/Ni alloys and the simulation results of ANFIS show that the established ANFIS model is suitable for the prediction of the mechanical properties of welded joints which can map the nonlinear relationship between the inputs and outputs with high accuracy of prediction, so the established ANFIS prediction model is effective.

Author Contributions: Conceptualization, Zhe Zou; Software, Juan Chen and Ming-Der Jean.

Acknowledgments: The authors gratefully acknowledge financial support from the Industry-University Cooperative Education Projects of the Ministry of Education (No.202102100020; No.202102391031), Undergraduate Education and Teaching Reform Research Project of Fujian Province (No. FBJG20220194) and Key Issues of Xiamen Humanities and Social Sciences Research Centre, 2024.

References

1. Suryanarayanan R. (1993). Plasma spraying: theory and applications. World scientific.
2. Sun G, Zhou R, Lu J, et al. (2015). Evaluation of defect density, microstructure, residual stress, elastic modulus, hardness and strength of laser-deposited AISI 4340 steel. Acta Materialia, 84: 172-189.
3. W.L. Wang, J.Q. Bi, S.R. Wang, K.N. Sun, M. Du, N.N. Long, Y.J. Bai. Microstructure and mechanical properties of alumina ceramics reinforced by boron nitride nanotubes. Journal of the European Ceramic Society. 31(13), 2011, 2277-2284.
4. Li XC, Stampfl J, Prinz FB (2000) Mechanical and thermal expansion behavior of laser deposited metal matrix composites of Invar and TiC. Mater Sci Eng A Struct 282:86–90.
5. Babout L, Brechet Y, Maire E, Fougeres R (2004) On the competition between particle fracture and particle decohesion in metal matrix composites. Acta Mater 52:4517–4525.

 doi:10.20944/preprints202404.1249.v1

6. Da Shu, Zhuguo Li, Ke Zhang, Chengwu Yao, Dayong Li, Zhenbang Dai. (2010). In situ synthesized high volume fraction WC reinforced Ni-based coating by laser cladding. Materials Letters 195 (2017) 178–181.
7. Zhang J, Lei J, Gu Z, et al. (2020). Effect of WC-12Co content on wear and electrochemical corrosion properties of Ni-Cu/WC-12Co composite coatings deposited by laser cladding. Surface and Coatings Technology, 393: 125807.
8. Chaokun Song, Xiaofei Liu, Fang Ye, Yongsheng Liu, Laifei Cheng. Mechanical and dielectric properties of SiCf/BN/SiBCN composites via different synthesis technologies. Journal of the European Ceramic Society. 39(14), 2019, 4417-4423.
9. Yu Pan, Yongsheng Liu, Mingxi Zhao, Ning Wang, Chenhao Wang, Sujun He, Fang Ye, Laifei Cheng. Effects of oxidation temperature on microstructure and EMI shielding performance of layered SiC/PyC porous ceramics. Journal of the European Ceramic Society. 39(15), 2019, 4527-4534.
10. Yamaguchi T, Hagino H. (2021). Effects of the ambient oxygen concentration on WC-12Co cermet coatings fabricated by laser cladding. Optics & Laser Technology, 139: 106922.
11. Cao Q, Fan L, Chen H, et al. (2022). Wear behavior of laser cladded WC-reinforced Ni-based coatings under low temperature. Tribology International, 176: 107939.
12. Chen Zishan, Li Hejun, Fu Qiangang, Qiang Xinfa.Tribological behaviors of SiC/h-BN composite coating at elevated temperatures. Tribology International 56 (2012) 58–65.
13. Andre Contin, Getúlio de Vasconcelos, Danilo Maciel Barquete, Raonei Alves Campos, Vladimir Jesus Trava-Airoldi, Evaldo José Corat. Laser cladding of SiC multilayers for diamond deposition on steel substrates. Diamond & Related Materials 65 (2016) 105–114.
14. H. Zhuang, L. Zhang, T. Staedler, X. Jiang, Nanoscale integration of SiC/SiO2 core-shellnanocables in diamond through a simultaneous hybrid structure fabrication, Appl. Phys. Lett. 100 (2012), http://dx.doi.org/10.1063/1.4712044.
15. Anjani Kumar, Anil Kumar Das. Evolution of microstructure and mechanical properties of Co-SiC tungsten inert gas cladded coating on 304 stainless steel. Engineering Science and Technology, an International Journal, 24(3), 2021, P 591-604.
16. A. Kumar, R. Kumar Ram, A. Kumar Das. Mechanical characteristics of Ti-SiC metal matrix composite coating on AISI 304 steel by gas tungsten arc (GTA) coating process. Mater. Today: Proc., 17 (2019), pp. 111-117.
17. Q. Li, G.M. Song, Y.Z. Zhang, T.C. Lei, W.Z. Chen, Microstructure and dry sliding wear behavior of laser clad Ni-based alloy coating with the addition of SiC, Wear. 254 (2003) 222-229. doi:10.1016/S0043-1648(03)00007-3.
18. S. Buytoz. Microstructural properties of SiC based hardfacing on low alloy steel. Surf. Coat. Technol., 200 (12-13) (2006), pp. 3734-3742.
19. F. Kretz, Z. Gácsi, J. Kovács, T. Pieczonka. The electroless deposition of nickel on SiC particles for aluminum matrix composites. Surf. Coat. Technol., 180-181 (2004), pp. 575-579.
20. Maolin Chen, Ling Pan, Xiaodong Xia, Wei Zhou, Yang Li. Boron nitride (BN) and BN based multiple-layer interphase for SiCf/SiC composites: A review.Ceramics International 48(23), Part A, 2022, 34107-34127
21. Richter J, Harabas K. (2019). Micro-abrasion investigations of conventional and experimental supercoarse WC-(Ni, Co, Mo) composites. International Journal of Refractory Metals and Hard Materials, 83: 104986.
22. A.K. Das et al. Effect of rare earth oxide (Y2O3) addition on alloyed layer synthesized on Ti-6Al-4V substrate with Ti+SiC+h-BN mixed precursor by laser surface engineering. Tribology International. 95, 2016, 35-43.
23. Mingxi Zhao, Yongsheng Liu, Nan Chai, Hailong Qin, Xiaofei Liu, Fang Ye, Laifei Cheng, Litong Zhang. Effect of SiBCN content on the dielectric and EMW absorbing properties of SiBCN-Si3N4 composite ceramics. Journal of the European Ceramic Society 38(4), 2018,1334-1340.
24. S. Mahdavi, F. Akhlaghi. Effect of the SiC particle size on the dry sliding wear behavior of SiC and SiC-Gr-reinforced Al6061 composites. J. Mater. Sci., 46 (24) (2011), pp. 7883-7894.
25. L. Li, H. Li, H. Lin, L. Zhuang, S. Wang, T. Feng, X. Yao, Q. Fu. Comparison of the oxidation behaviors of SiC coatings on C/C composites prepared by pack cementation and chemical vapor deposition. Surf. Coat. Technol., 302 (2016), pp. 56-64.
26. Xiangming Li, Litong Zhang, Xiaowei Yin, Liyun Feng, Quan Li. Effect of chemical vapor infiltration of SiC on the mechanical and electromagnetic properties of Si3N4–SiC ceramic.Scripta Materialia. 63(6), 2010, 657-660.
27. Yunyu Li, Lingjun Guo, Qiang Song, Hejun Li, Qiangang Fu, Kezhi Li. Oxidation pre-treatment and electrophoretic deposition of SiC nanowires to improve the thermal shock resistance of SiC coating for C/C composites. Journal of Alloys and Compounds. 636(5) 2015, 165-170.
28. Shuang Yin, Yuhang Jiang, Kai Su, Xia Fang, Yang Wang, Quan Li, Jian Yang. Preparation, mechanical, dielectric and microwave absorption properties of hierarchical porous SiCnw-Si3N4 composite ceramics. Journal of the European Ceramic Society. 42(9), 2022, 3820-3830.

29. Wei Zhou, Lan Long, Yang Li. Mechanical and electromagnetic wave absorption properties of Cf-Si3N4 ceramics with PyC/SiC interphases. Journal of Materials Science & Technology. 35(12), 2019, 2809-2813.
30. Subhrojyoti Mazumder, Hendrik Simon Cornelis Metselaar, Nazatul Liana Sukiman, Nurin Wahidah Mohd Zulkifli. Friction and wear behavior of fluoride added Si3N4-SiC ceramic composites at elevated temperature. Ceramics International 49(8), 2023, 12787-12795.
31. F. Lusquiños, J. Pou, F. Quintero, M. Pérez-Amor. Laser cladding of SiC/Si composite coating on Si-SiC ceramic substrates. Surf. Coat. Technol., 202 (9) (2008), pp. 1588-1593.
32. B.J. Zheng; X.M. Chen; J.S. Lian. Microstructure and wear property of laser cladding Al+SiC powders on AZ91D magnesium alloy. Optics and Lasers in Engineering.2010, 48 (5)526-532.
33. Xiaoli Sun, Jiakai Zhang, Weiguo Pan, Wenhuan Wang, Congwei Tang. A review on the preparation and application of BN composite coatings. Ceramics International. 49(1), 2023,24-39.
34. Neng Li; Yi Xiong; Huaping Xiong; Gongqi Shi; Jon Blackburn;Wei Liu; Renyao Qin. Microstructure, formation mechanism and property characterization of Ti+SiC laser cladded coatings on Ti6Al4V alloy. Materials Characterization. 2019, 148,43-51.
35. J.D. Majumdar, B.R. Chandra, A.K. Nath, I. Manna. Laser composite surfacing of stainless steel with SiC.Phys. Stat. Sol. (a), 203 (9) (2006), pp. 2260-2265.
36. S.P. Lee et al. Fabrication of liquid phase sintered SiC materials and their characterization. Fusion Engineering and Design. 81(8-14) 2006, 963-967.
37. Shu D, Li Z, Zhang K, et al. (2017). In situ synthesized high volume fraction WC reinforced Ni-based coating by laser cladding. Materials Letters, 195: 178-181.
38. F. Rebillat, J. Lamon, A. Guette, The concept of a strong interface applied to SiC/SiC composites with a BN interphase, Acta Mater. 48 (2000) 4609–4618.
39. Jens Eichler, Christoph Lesniak. Boron nitride (BN) and BN composites for high-temperature applications. Journal of the European Ceramic Society. 28(5), 2008, 1105-1109.
40. Lotfi A Zadeh. Fuzzy logica personal perspective. Fuzzy Sets and Systems, 281:4–20, 2015.
41. J Lee, K Um. A comparison in a back-bead prediction of gas metal arc welding using multiple regression analysis and artificial neural network. Optics and Lasers in Engineering,34(3) 2000, 149-158.
42. Sukhomay Pal, Surjya K. Pal, Arun K. Samantaray. Artificial neural network modeling of weld joint strength prediction of a pulsed metal inert gas welding process using arc signals. Journal of Materials Processing Technology. 202(1-3), 2008, 464-474.
43. D.S. Nagesh, G.L. Datta. Prediction of weld bead geometry and penetration in shielded metal-arc welding using artificial neural networks. Journal of Materials Processing Technology. 123(2) 2002, 303-312.
44. C.R.Wang, Z.Q. Zhong, M. D. Jean. Effect of ingredients proportions on mechanical properties in lasercoated WC-blend welds. Phys. Scr. 99 (2024) 035945. https://doi.org/10.1088/1402-4896/ad2759
45. Nicola Contuzzi; Giuseppe Casalino. On modelling Nd:Yag nanosecond laser milling process by neural network and multi response prediction methods. Optik - International Journal for Light and Electron Optics.2023,284: 170937-
46. Meng Liu; Chunzheng Duan; Guohe Li; Yujun Cai; Feng Wang; Lei Li. Multi-response optimization of Ni-based laser cladding via principal component analysis and grey relational analysis. Optik-International Journal for Light and Electron Optics. 2023.287
47. Liu, J C;Ni, L B.Prediction of laser clad parameters based on neural network. Materials Technology: Advanced Performance Materials.012, 27 (1),11-14
48. Zhou, Zhijie; Du, Yanbin; He, Guohua; Xu, Lei; Shu, Linsen. Optimization and Characterization of Laser Cladding of 15-5PH Coating on 20Cr13 Stainless Steel. Journal of Materials Engineering and Performance. 2023, 32 (3) 962-977.
49. Gao, Jiali;Wang, Chi;Hao, Yunbo;Liang, Xudong;Zhao, Kai. Prediction of TC11 single-track geometry in laser metal deposition based on back propagation neural network and random forest. Journal of Mechanical Science and Technology. 2022, 36 (3)1417-1425.
50. Liaoyuan Chen, Tianbiao Yu, Xin Chen, Yu Zhao, Chuang Guan. Process optimization, microstructure and microhardness of coaxial laser cladding TiC reinforced Ni-based composite coatings. Optics & Laser Technology, 152, 2022, 108129. https://doi.org/ 10.1016/j.optlastec.2022.108129
51. Rasool Saeedi, Reza Shoja Razavi, Saeed Reza Bakhshi, Mohammad Erfanmanesh, Ahmad Ahmadi Bani. Optimization and characterization of laser cladding of NiCr and NiCr-TiC composite coatings on AISI 420 stainless steel. Ceramics International. 47(3), 2021, 4097-4110.
52. Jang J S R. ANFIS: Adaptive-Network–Based Fuzzy Inference System. IEEE Transactions on Systems, Man, and Cybernetics,1993, 23(3): 665–685.
53. Lan-Ling Fu; Jin-Shui Yang; Shuang Li; Hao Luo; Jian-Hao Wu. Artificial neural network-based damage detection of composite material using laser ultrasonic technology. Measurement.2023,220,113435-
54. Muhammad Arif Mahmood, Andrei C. Popescu, Mihai Oane, Asma Channa, Sabin Mihai, Carmen Ristoscu, Ion N. Mihailescu. Bridging the analytical and artificial neural network models for keyhole

 doi:10.20944/preprints202404.1249.v1

formation with experimental verification in laser melting deposition: Anovel approach. Results in Physics. 26, 2021, 104440.
55. Andenson K,Cook G E,Karsai G et al. Artificial neural network applied to arc welding process modeling and control. IEEE Trans on Industry Application◎1990◎26(5):824-830.
56. S. Chowdhury, S. Anand. Artificial neural network based geometric compensation for thermal deformation in additive manufacturing processes. Int. Manuf. Sci. Eng. Conf, Blacksburg, VA, USA (2016).
57. W. Sudnik, D. Radaj, W. Erofeew. Computerized simulation of laser beam welding, modelling and verification. J Phys D Appl Phys, 29 (11) 1996, 2811-2817.
58. Yuhang Zhang, Yifei Xu, Yaoning Sun and Wangjun Cheng. Surface quality optimization of laser cladding based on surface response and genetic neural network model. Surface Topography: Metrology and Properties, 10(4)2022, 10 044007.
59. S. Genna, E. Menna, G. Rubino, F. Trovalusci. Laser machining of silicon carbide: Experimental analysis and multiobjective optimization. Ceramics International 49(7), 2023,10682-10691.